Functional and structural analyses of the terminal organelle of *Mycoplasma genitalium*

Luis González González

2015

Doctoral dissertation submitted to fulfil the requirements to obtain the Doctor of Phylosophy Degree in Bioquímica, Biologia Molecular i Biomedicina at Universitat Autònoma de Barcelona

This work has been performed at the Institut de Biotecnologia i Biomedicina in the Departament de Bioquimica i Biologia molecular under the supervision of Dr. Jaume Piñol Ribas and Dr. Enrique Querol Murillo

5. Chapter II: Functional analysis of the protein encoded in MG_318 locus: P32

5.1 Introduction

5.1.1 Previous knowledge of P32 protein

Although the orthologous of P32, P30, has been extensively studied in *M. pneumoniae* little is known of *M. genitalium* P32 protein. The single experiment available in the literature reveals that P32 is capable of restoring the phenotype caused by the absence of P30thus demonstrating its homology by experimental procedures (Relich and Balish, 2011). This fact is particularly striking given its sequence similarity is not high in particular regions of the protein (Fig. 2.1A). Both P32 and P30 are thought to be cytadhesins. The establishment of this role in *M. pneumoniae* was performed in a spontaneous frameshift mutant called II-3 (Fig. 2.1B).

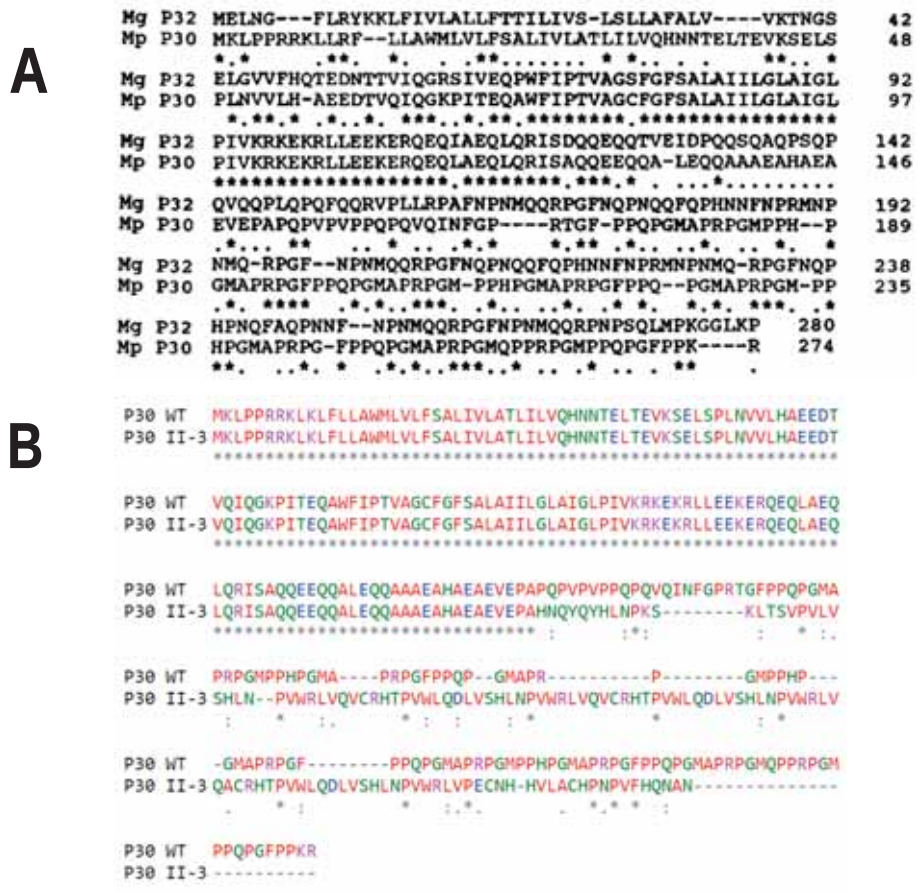

Figure 2.1. Sequence comparison at amino acid level of P32 and P32 variants. **A.** Sequence comparison between P32 and P30. **B.** Sequence comparison of P30 in WT strain andII-3 strain.

Therefore mutant II-3 presents a modified version of 31.5 kDa that only shares sequence identity from amino acid 1 till amino acid 151. Authors claimed that mutant II-3 is equal to a null mutant for P30 protein because no signal of P30 protein is detected when using a polyclonal antibody generated against residues from 102 to 181 of the protein (Layhschmitt and Herrmann, 1994, Romero-Arroyo et al., 1999). The phenotype analyses of strain II-3 showed that cells of this strain were unable to attach erythrocytes but are capable to adhere to glass surfaces. Gliding motility was impossible under this genetic background. It is important to note that although it has been suggested that the P30 variant in II-3 is unstable there is no definitive data about that. Morphology of mutant II-3 was more ovoid and pleomorphic than the filamentous morphology of WT strain suggesting also a role of P30 in proper cell development. Complementation assays demonstrated that the II-3 P30 variant is the responsible of gliding, cytadhesion and morphology defects in this strain. After several passages of strain II-3, a revertant frameshift mutation lead to the expression of P30 protein that differs in amino acid sequence from residues 135 to 151. This region showed to be critical for gliding velocity but not for cytadhesion (Hasselbring et al., 2005). Moreover, a mutant with a partial deletion of the proline and glutamine rich repeats in the C-ter of P30 revealed that this region is critical for adhesion and motility, with higher affectations in cytadhesion capacity than the 135-151 variant but lesser in when compared to the II-3 strain (Hasselbring et al., 2005). Latter analyses showed that P30 is a protein that requires posttranslational cleavage for proper gliding activity and hemadsorption activity (Chang et al., 2011b). Topology predictions show that P32 and P30 present a signal peptide and a transmembrane region in the N-ter of the protein separated by 19 aa. Those 19 aa have also been showed to be essential for gliding activity and cytadherence (Chang et al., 2011a). Noteworthy is the fact that deletions in the area of the frameshift present in strain II-3 also lead to a complete destabilization of P30 (Chang et al., 2011a). It has also been demonstrated that P65 protein is destabilized in the absence of P30 (Chang et al., 2011a).

5.2 Results

5.2.1 Recombinant expression of P32 and polyclonal antibody generation

The recombinant expression in *E. coli* of P32 protein was planned to obtain polyclonal antisera of P32 protein. Since Trp68 is coded by a TGA codon that leads to a stop codon in *E.coli* a directed mutagenesis by PCR was performed to exchange TGA for TGG. Later, it was cloned in a pET-21d and transformed in BL21De3 cells. Several temperatures, times and induction conditions were tested but no expression or purification products were detected (data not shown). Almost certainly, the signal peptide and the transmembrane predicted segments are the responsible of the poor expression of P32 protein in *E. coli*. For this reason a shorter version of MG318 gene was cloned in the same pET-21d plasmid. This new version contains the coding sequence from amino acid 93 till 280.That region was selected because does not contain either the signal peptide or the transmembrane region (Fig. 2.2).

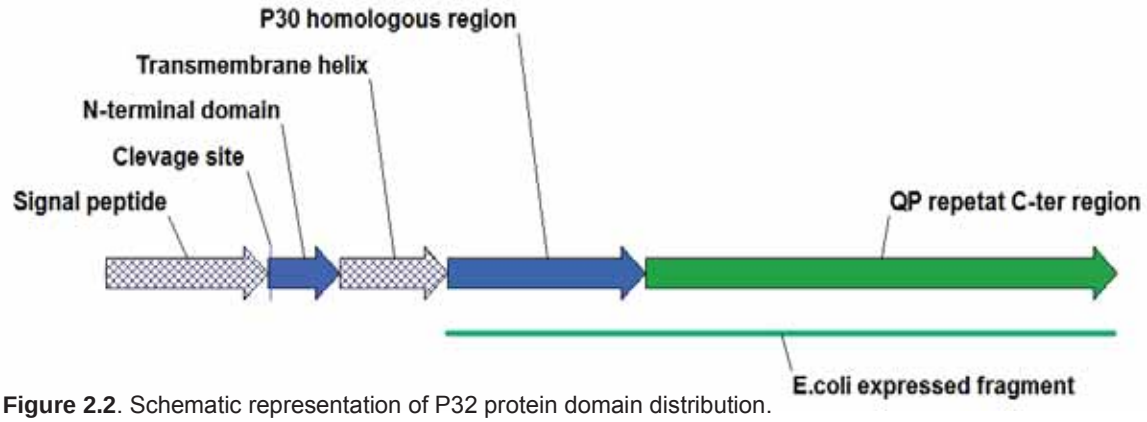

Figure 2.2. Schematic representation of P32 protein domain distribution.

In this case the recombinant expression at 37°C 3h yielded to moderated amounts of the C-ter region of P32 protein (Figure 2.3). Although a 37 kDa intense band could be observed after inducing recombinant expression two bands around 27 kDa (the expected molecular weight for the C-terminal cloned in the pET-21d was 23 kDa).

It is possible that this higher-than-expected Mw is due to aberrant electrophoretic mobility as a result of its extraordinary content in prolines (John and Keller, 1995, Pham and Sivasubramanian, 1992). It is also noticeable the apparition of a 26 and 27 kDa bands after the addition of the inductor to the media.

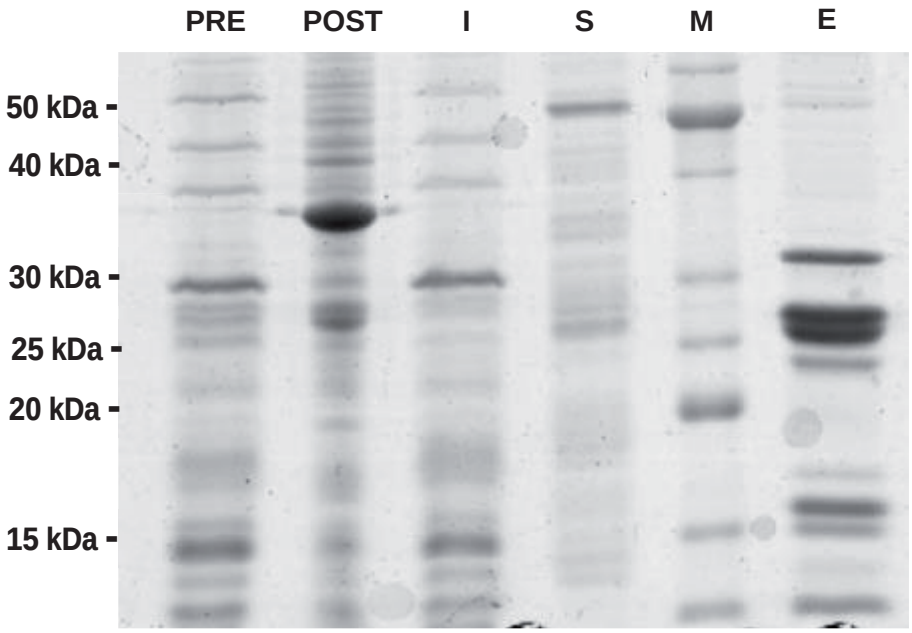

Figure 2.3. SDS-PAGE of recombinant expression and purification of P32 in *E.coli* BL21(DE3) cells . M: molecular weight marker. Benchmark ladder (Life technologies), PRE: sample of the culture before induction. POST: sample of the culture after induction S: soluble fraction after cell lysis. I. insoluble fraction after cell lysis E: eution at 500 mM of imidazole. Fraction size is 0.5 ml.

The three most intense bands—31 kDA, 26 kDa and 25 kDa— that were recovered in the elution process of the purification were further evaluated. Fingerprint mass-spectrometric (MALDI-TOF) analyses of these three bands showed yielded peaks with good correlation to the theoretical peaks of C-ter of P32 (data not shown).

After dialysis in PBS recombinant P32 protein was intraperitoneally injected in BALB/c mice. Once the immunisation protocol was finished serum was tested to be positive against P32 protein (see section 5.2.3).

5.2.2 Plasmids for obtaining a P32 null mutant, a P32 C-ter lacking mutant and to reintroduce the WT allele

In order to study the function of P32 protein in *M. genitalium*, plasmid pΔMG318 was designed and obtained (Fig. 2.4A). This plasmid harbours a cat gene under the control of MG_438 promoter flanked by 1 kb homology regions. Once electroporated, this plasmid can lead to a null mutant for MG_318 gene if a double recombination event is performed by homologous recombination. The homology regions were designed to keep the last 129 bp at the 3' of the MG_318 gene because it is feasible that the promoter of MG_317—which is only 14 pb downstream of the stop codon of MG_318—would lie within this region (see Fig. 2.8). Hence the resulting strains will be named ΔMG318.

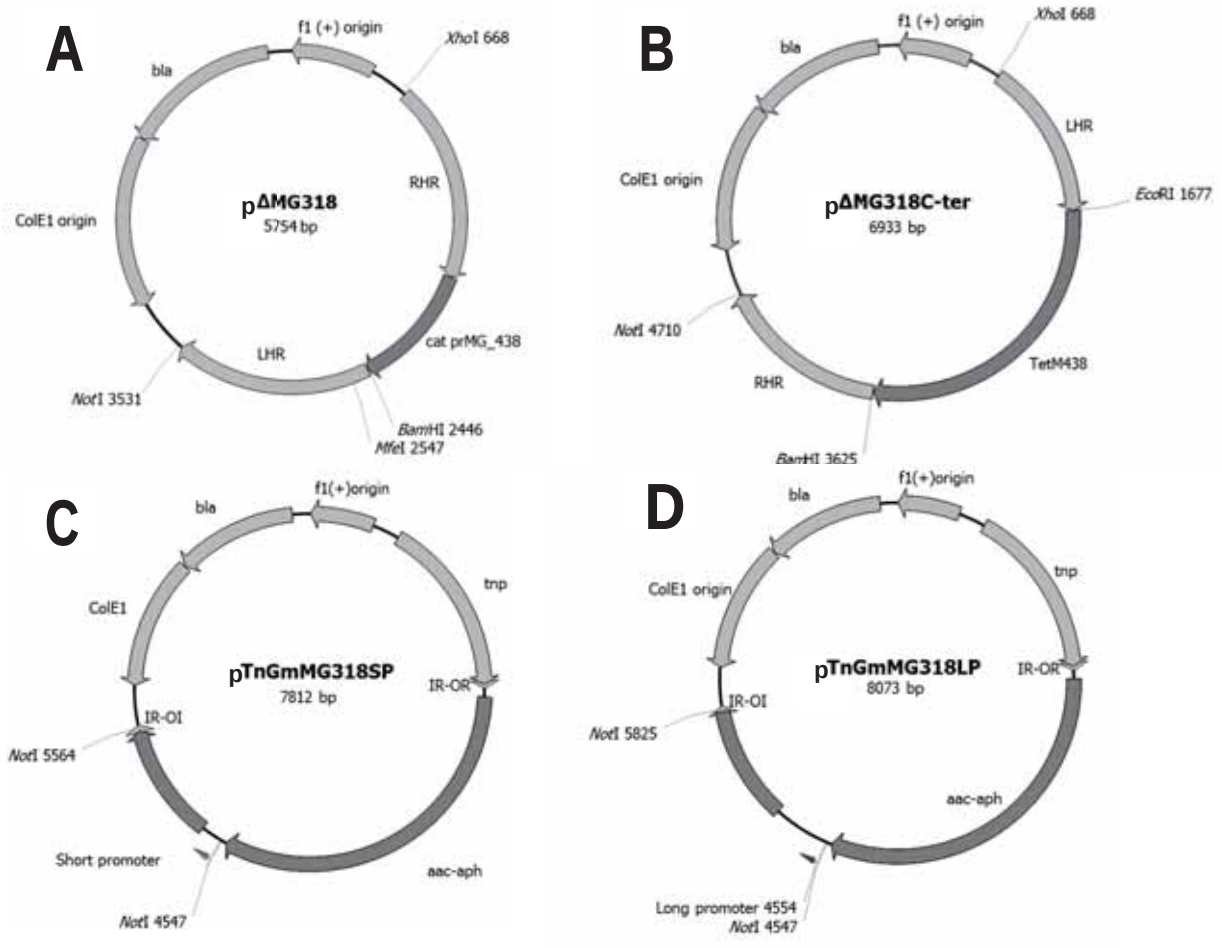

Figure 2.4. Schematics of plasmids designed for introducing MG318 mutations or introductions in the genome. **A.** pΔMG318. **B.** pΔMG318C-ter. **C.** pTnGmMG318SP**D.** pTnGmMG318SP. Relevant restriction site for plasmid generation are marked.

Due to the possibility that strain II-3 is still expressing an aberrant frameshift-generated P30 form, a reproduction of that mutation was aimed to be achieved in *M. genitalium*. Unluckily, the same frameshift mutation is not possible in *M. genitalium* because of an apparition of a stop codon after 20 bp of the deleted base. For this reason we generated pΔMG318C-ter which contains two 1 kb regions flanking a tetracycline resistance gene under the promoter of MG_438 (Figure 2.4B). Once transformed into *M. genitalium* cells, pΔMG318C-ter plasmid will delete the P32 C-terminal region from amino acid Q151, right in the same position as the frameshift mutation described in *the* P30 protein of *M. pneumoniae*. The homology regions in this plasmid were also designed to keep the last 129 pb upstream of MG_317 gene. The strains generated by this plasmid will be called ΔMG318C-ter.

For later reintroduction of MG_318 WT allele into ΔMG318 or ΔMG318C-ter to demonstrate that phenotype observed in those strains is solely consequence of the intended deletion, pTnGmMG318SP and pTnGmMG318LP were built (SP means short promoter and LP means long promoter, Fig. 2.4C and Fig.2.4D). All previous works performed in *M.pneumoniae* (Romero-Arroyo et al., 1999, Chang et al., 2011b, Chang et al., 2011a) and *M. genitalium* (chapter II) for introducing the WT allele or mutated ones in the genome by transposition carried a promoter of 750 bp that also includes the upstream gene and its promoter. Hence, to avoid the possible overexpression of MG_319 gene when reintroducing the WT in ΔMG318 and ΔMG318C-ter strains two different constructs were generated. The longer one presents 427 bp upstream of MG318 including neither the translation start codon of MG_319 nor its promoter sequence. The shorter version of MG318 promoter only included 166 bp upstream of the MG318 gene. Those 166 bp does not include any ATG codon, aiming to minimize the number of possible artefactual ORFs generated by the introduction of the transposon harbouring MG318 under the control of this short promoter.

5.2.3 Confirmation of MG318 mutants

Western blot analysis, using the antiserum generated in section 5.2.1, revealed that not all the recovered clones exhibited the expected phenotype (Figure 2.5A and 2.5B) most likely caused by a single recombination event. No signal was detected for many of the clones recovered after transformation with pΔMG318 but two major bands (34 kDa and 27 kDa) were detected. The expected bands are 32 kDa for the full-length protein and 27 kDa for the processed protein. Densitometry analyses showed the 34 kDa band is three times less intense than the 27 kDa. In addition, a high number of lower intensity bands was also observed, suggesting a quick turnover or a short half-life of P32 protein. A diffuse low-intensity band of 13 kDa was observed in most of the clones recovered after de transformation with pΔMG318C-ter. The expected band for the C-ter deletion of P32 (after the putative proteolytic cleavage) is 12 kDa. Attempts to further focalize this diffuse bands with Tricine-SDS-PAGE system (Schagger, 2006) did not show better results (data not shown). Interestingly, SDS-PAGE profiles showed that almost half of the clones lacking P32 presented a complete loss of P110 and P140 adhesins, while the other half presented only a reduction of a 60% in the level of those proteins. Clone 10 was randomly selected for further analyses and will be further referred as Δmg318. However, all of the clones presenting a deletion of the C-ter of P32 did present a decrease of P110 and P140 levels ranging from 60% to 40% except for one clone that showed WT levels. This latter clone resulted to be a single crossover event and was not further analysed. Within the clones having reduced levels of the mutants lacking the C-ter of P32, clone 10 was chosen further genotypic and phenotypic assays—because of its reduced loss of P110 and P140—and will be referred as and Δmg318C-ter.

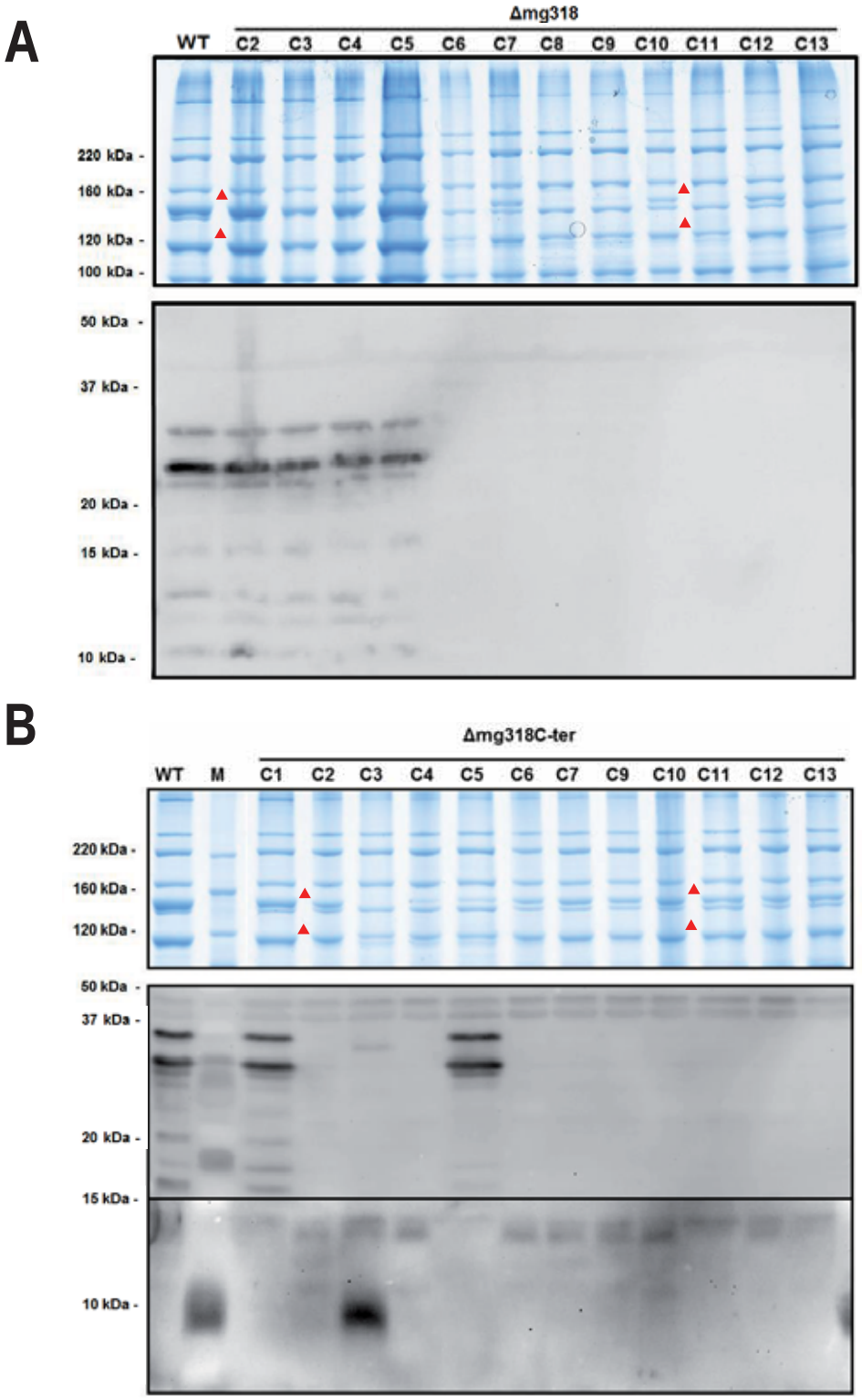

Figure 2.5. Protein profiles by SDS-PAGE and Western blots of MG_318 related strains. **A.** Different individual colonies recovered and analysed that have been electroporated with pΔMG318. **B.** Different individual colonies recovered and analysed that have been electroporated with pΔMG318C-ter. Different contrast was applied for the upper and the lower part of the western blot for clarity purposes. Lower vertices of the red triangles indicate the position of P140 and P110. In all cases no effect on the levels of MG218 and M312 where observed. Reduced levels of MG386 can be observed in the absence of P110 and P140. Strains with reduced levels of the main adhesins showed a slightly reduced levels of MG386.

SDS-PAGE (Fig. 2.5) and western blot analyses of Δmg318 and Δmg318C-ter strains using antisera against most of the known proteins of the terminal organelle (Fig. 2.6) show that those strains present identical levels of all the proteins analysed except from reduced levels of P110 and P140.

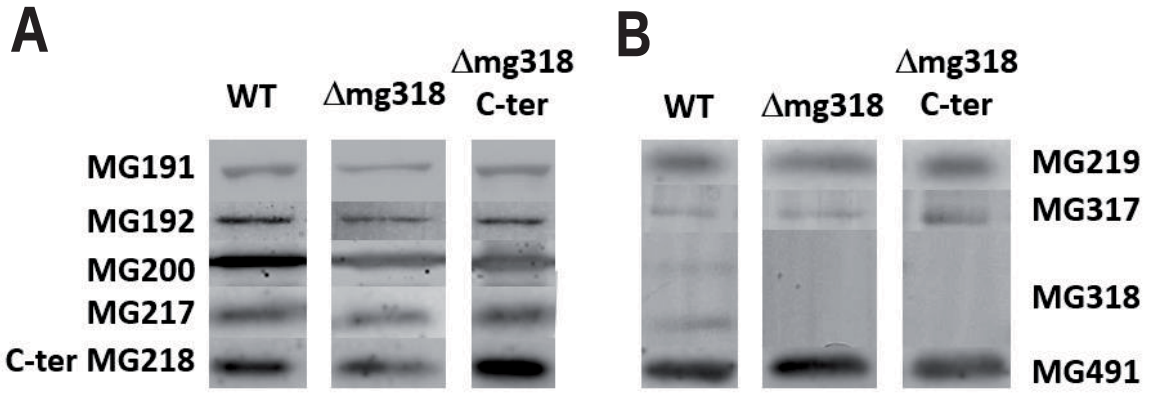

Figure 2.6. Western blot from WT and Δmg318 mutant strains using antisera against terminal organelle proteins.

Both plasmids pTnGmMG318SP and pTnGmMG318LP proved to be equally functional (Figure 2.7) restoring P32 levels. Clones with diminished adhesin levels recovered WT amounts after the reintroduction of the WT allele (Fig. 2.7). As an *exempli gratia* of Δmg318 strains lacking P110 and P140 the genome of Δmg318 c9 was also analysed by complementation studies and sequencing analyses. Δmg318 c9 did not recover adhesins levels at all when reintroducing P32 WT allele (Fig. 2.7). This results suggest MG_318 deletion is not the only genome modification those strains. Only mutants obtained with the transformation by pTnGmMG318SP were further analysed.

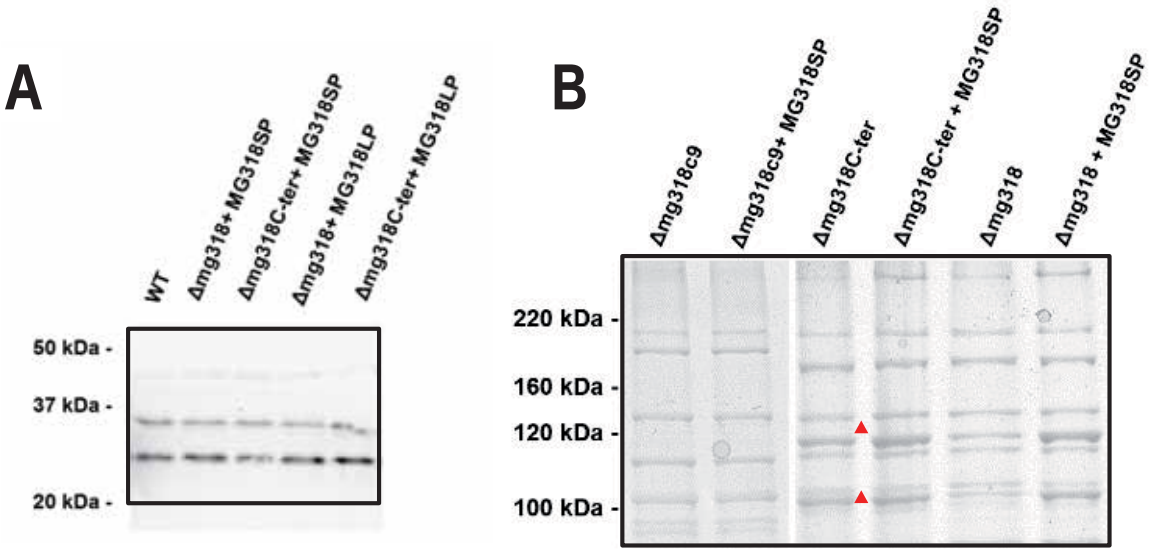

Figure 2.7. Western blots and protein profile of the WT and some P32 related strains. **A.** Western blot using P32 antiserum **B.** SDS-PAGE showing the high molecular weight proteins of the analysed strains.

Whole genome sequencing of the genome of Δmg318 and Δmg318C-ter and Δmg318 c9 mutant strains were performed. All mutant strains lead to the intended gene replacement (Fig. 2.8, Figure 2.9 and data not shown). Comparison of the reads obtained against the wild-type genome demonstrates that not a single read of MG_318 or MG_318C-ter, corroborating the clonal purity of these strains. Additionally, comparison with the expected genomes after double recombination events showed the proper gene replacement with no further mutations in the region.

Comparative variant analyses of the coding region for P110 and P140 of Δmg318 c9, Δmg318 c10 and Δmg318 c10 showed significant differences in the SNPs of this region in all strains (Fig. 2.10). Despite of the fact that the AGT repeat variance that is common in all strains, Δmg318 c9 show a high degree of variability in regions RC1, RC2 and RC3. No significant differences were observed in any other regions of the genome except for the MgPa islands[4].

[4] For detailed information about all the SNPs detected see appendix in section 12.4.

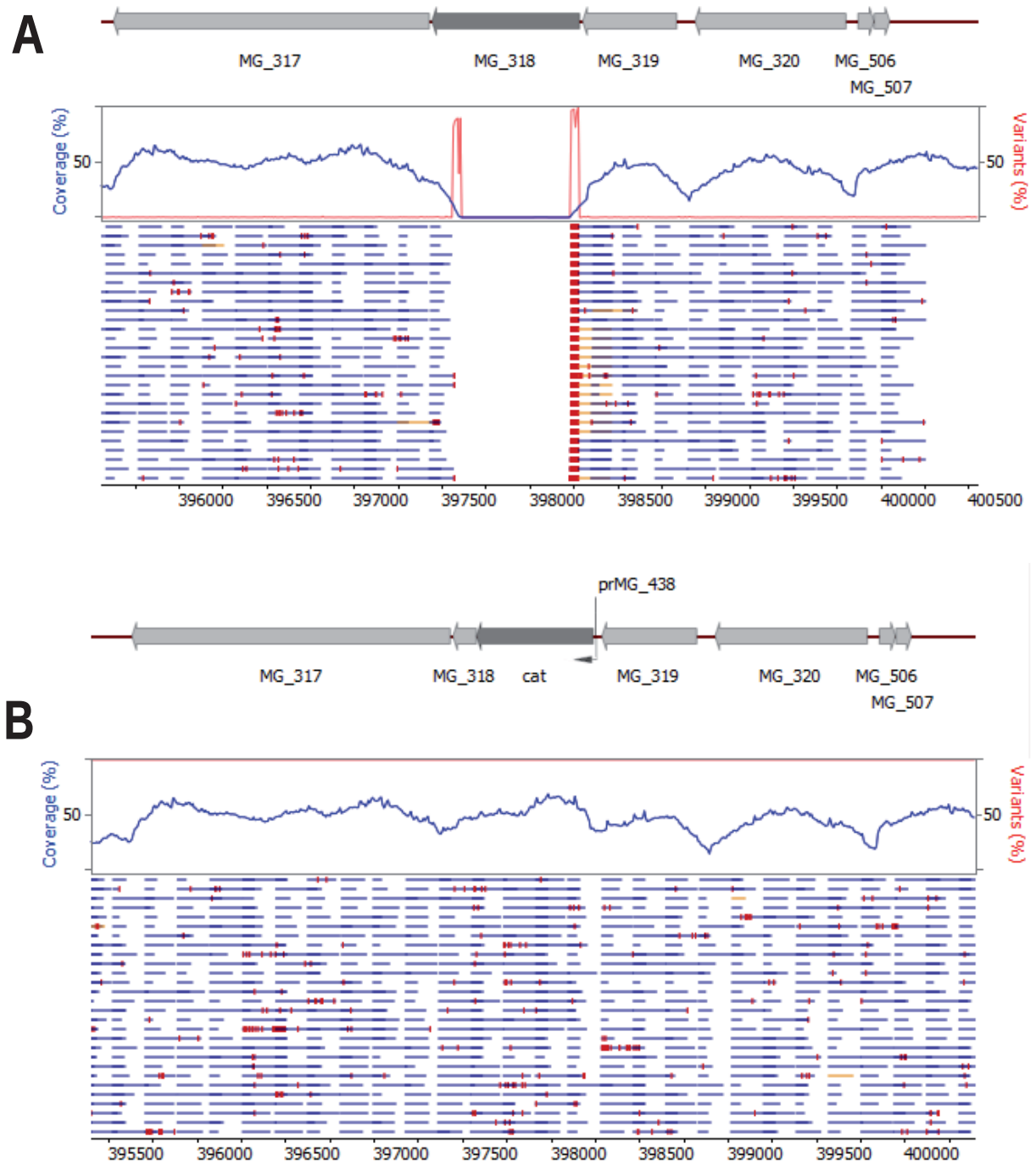

Figure 2.8. Region of the whole genome analysis of Δmg318 strain. **A.** Comparison with the genome of G37 wild type strain. **B.** Comparison with the theoretical genome of Δmg318 strain. The numbers indicate base numbers of reference genome used.

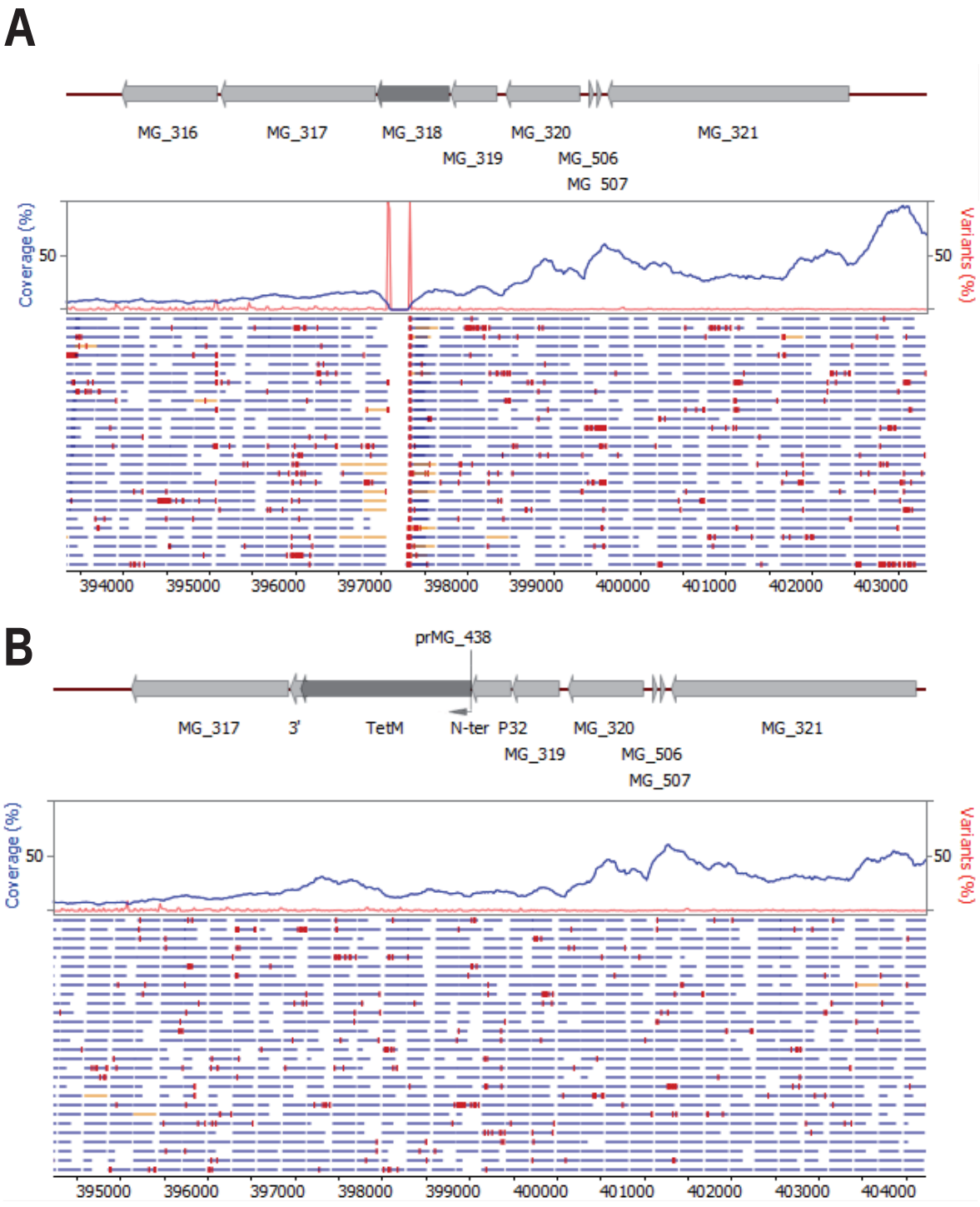

Figure 2.9. Region of the whole genome analysis of Δmg318 strain. **A.** Comparison with the genome of G37 wild-type strain. **B.** Comparison with the theoretical genome of Δmg318C-ter strain. The numbers indicate base numbers of reference genome used.

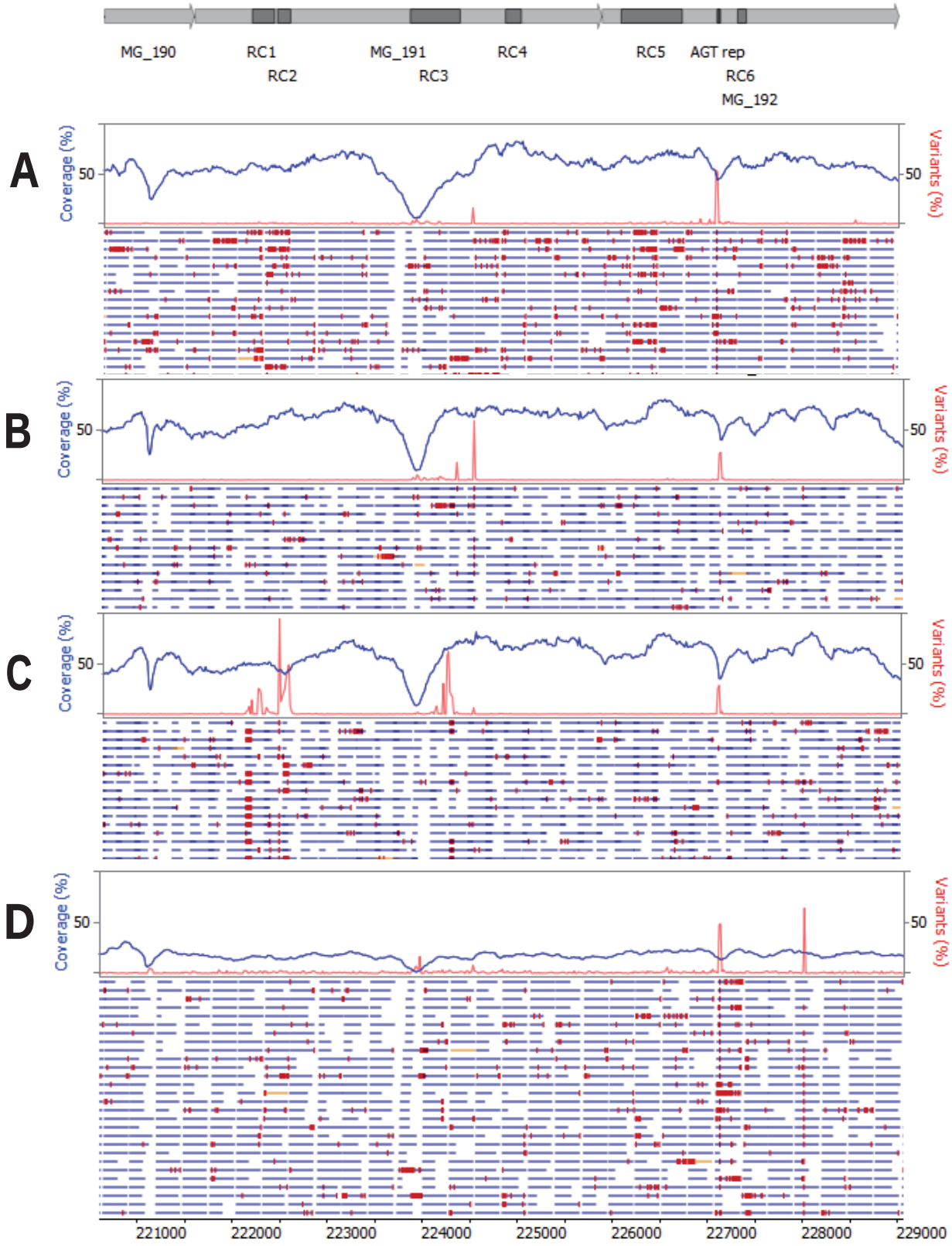

Figure 2.10. Genetic variation of MgPa operon in WT and MG_318 mutant strains. Sequence comparisons used WT as reference genome **A.** G37 wild-type strain. **B.**Δmg318 strain clone 10. **C.** genome of Δmg318 strain clone 9. **D.** Δmg318C-ter c10.

5.2.4 Characterization of P32 mutants

5.2.4.1 Gliding motility

Gliding motility parameters of the designed strains in this chapter were qualitatively and quantitatively analysed and compared. MG_318 mutants revealed a strong implication of P32 in gliding motility velocity, frequency and behaviour (Figure 2.11).

No statistical differences in the ratio of circular and erratic tracks were observed (Figure 2.12A). Quantitative analysis of gliding parameters of Δmg318 cells showed a decrease of a 43 % in gliding frequency (34% vs 77%) and a decrease of a 61% in gliding speed (0.070 ± 0.004 μm s^{-1} vs 0.112 ± 0.004 μm s^{-1}) when compared with the WT.

In addition, a 58% increase of the diameter of the depicted circular tracks is significantly different (0.148 ± 0.058 μm vs 0.932 ± 0.627 μm). Those analyses also revealed that the gliding phenotype of strains lacking P32 and P32 C-ter are not significantly distinct and were fully restored when reintroducing the WT allele in both strains (Figure 2.12).

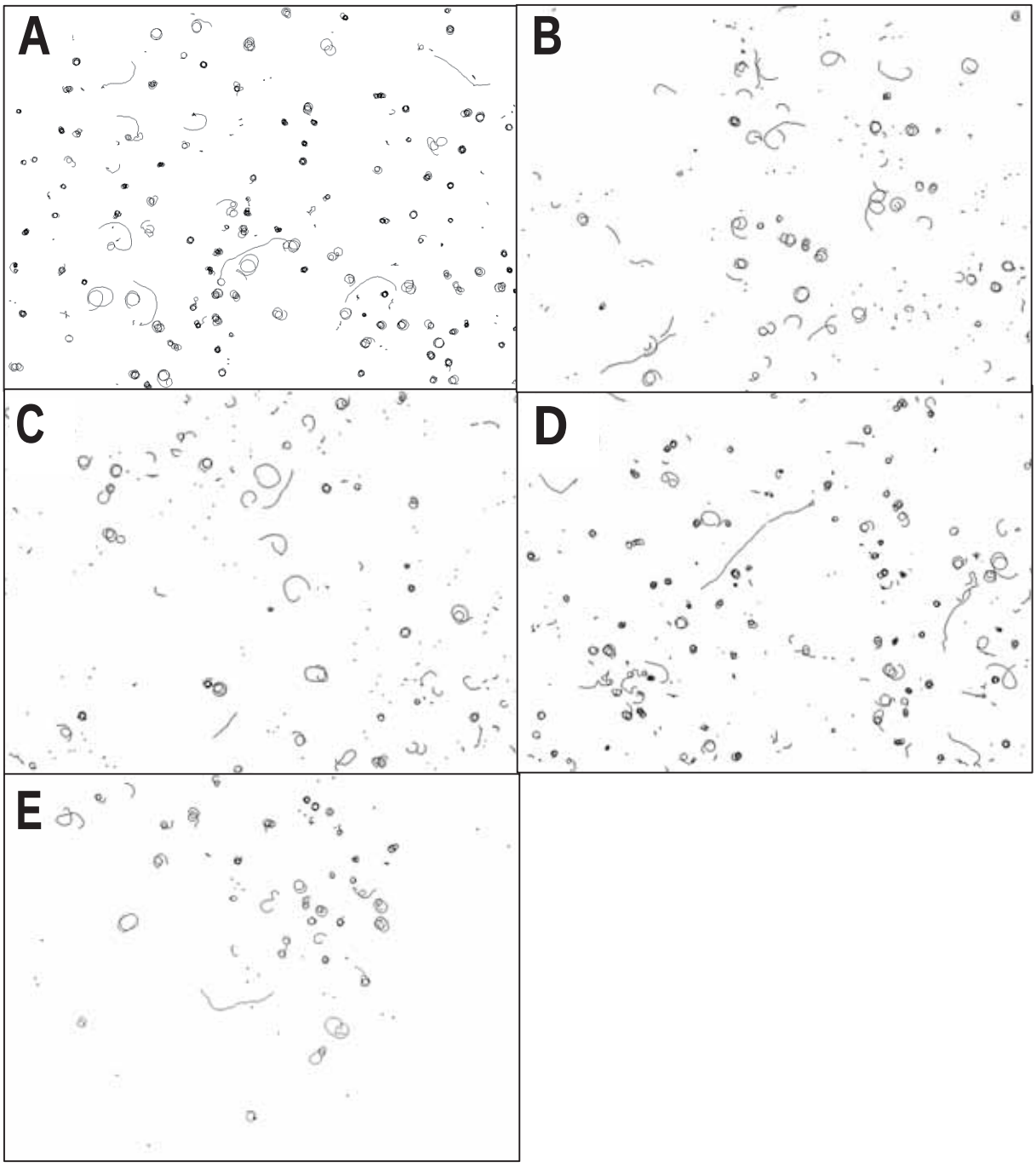

Figure 2.11. Paths depicted by MG318mutant strains in comparison with WT strain during a period of two minutes at 37ºC in SP4 medium. **A.** WT **B.** Δmg318 **C.** ΔMG318C-ter **D.** Δmg318 + MG318SP **E.** ΔMG318 C-ter + MG318SP. Each image shows a region of 86.9 x 65.2 μm.

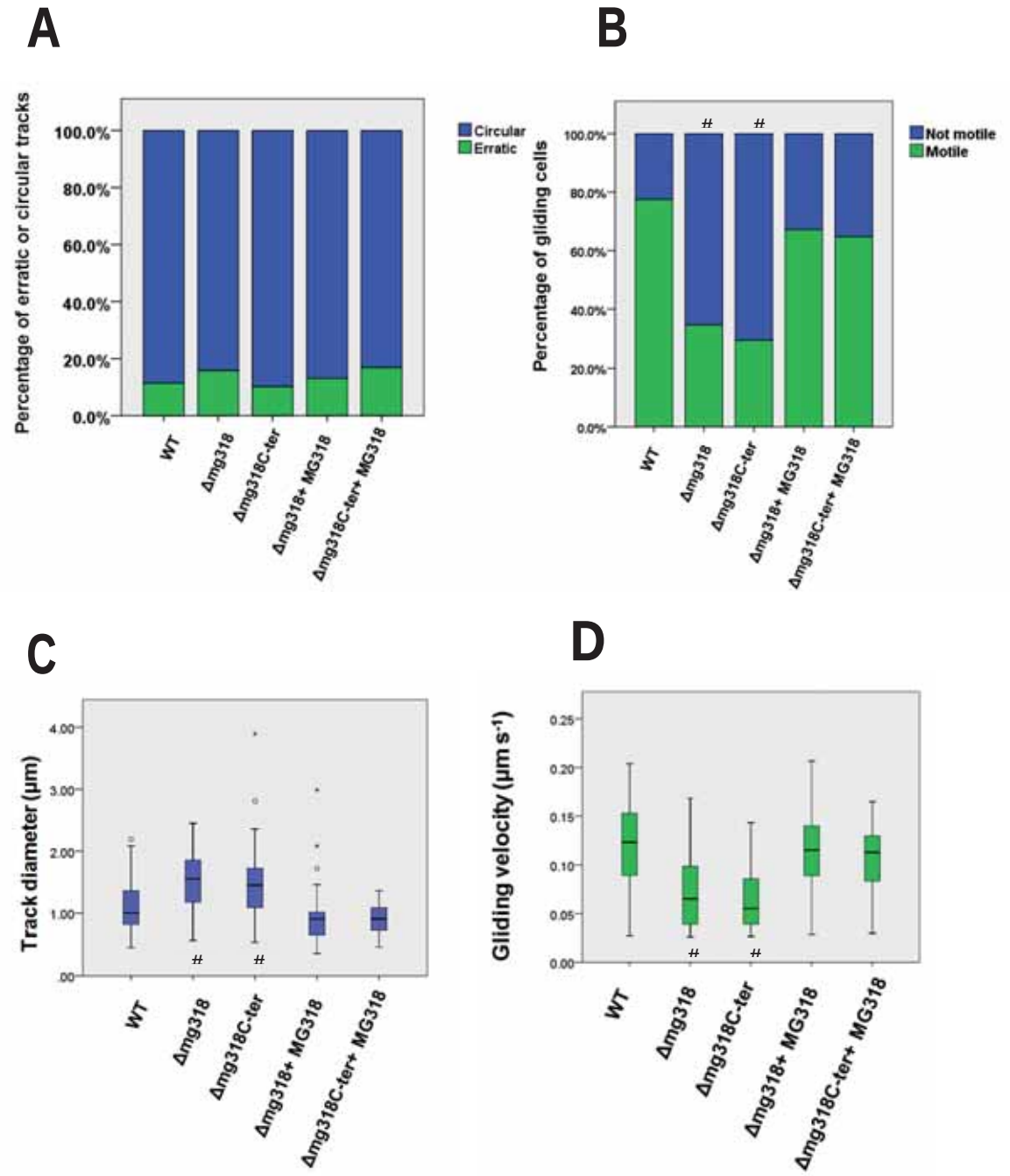

Figure 2.12. Gliding properties of WT and strains with modifications related to MG_318. **A.** Frequency of erratic and circular tracks **B.** Frequency of motile and non-motile cells **C.** Boxplots of gliding velocity. The number sign (#) indicates statistical significantly different when compared with the WT (*p*-value < 0.01).

5.2.4.2 Cellular morphology

Cellular morphology of cells lacking P32 or P32 C-ter was assessed by scanning electron microscopy (Fig. 2.13). The most striking feature of these strains is the low number of individual cells present in the sample. In contrast, most of the cells in these strains belong to multiple cell aggregates frequently linked by one or more thin and long filaments. Quantitatively, a decrease of a 36% of individual cells (83% vs 47%) is detected. An increase of a 33% of the cells clumped together was also observed (33% vs 5%). No other remarkable effects such as cells with multiple terminal organelles or a frequency increase of the number of cells found in normal cell division were detected. As equally observed in the gliding properties previously analysed, no statistical differences were observed between the strain lacking P32 or P32C-ter (Fig. 2.14A).

Moreover, individual cells showed the standard WT flask-shape morphology, but detailed analyses of the shape of the terminal organelle revealed significant differences (Figure 2.13B). Although the difference in the shape of the terminal organelle is subtle, the bulging end of the TO corresponding to the terminal button is not present in any of the cells in Δmg318 or Δmg318C-ter strains. 99% of Δmg318 or Δmg318C-ter cells presented this phenotype but only 18% of the cells of the WT strain showed that terminal button morphology. This anomalous terminal button will be further called 'smaller terminal button'. The presence of a 12% of cells with a thicker terminal organelle in strains lacking either P32 or P32C-ter is also remarkable. All of these differences were supported by statistical analyses. Complementation assays with MG_318SP (Figure 2.14B) and data not shown) restored wild-type morphology.

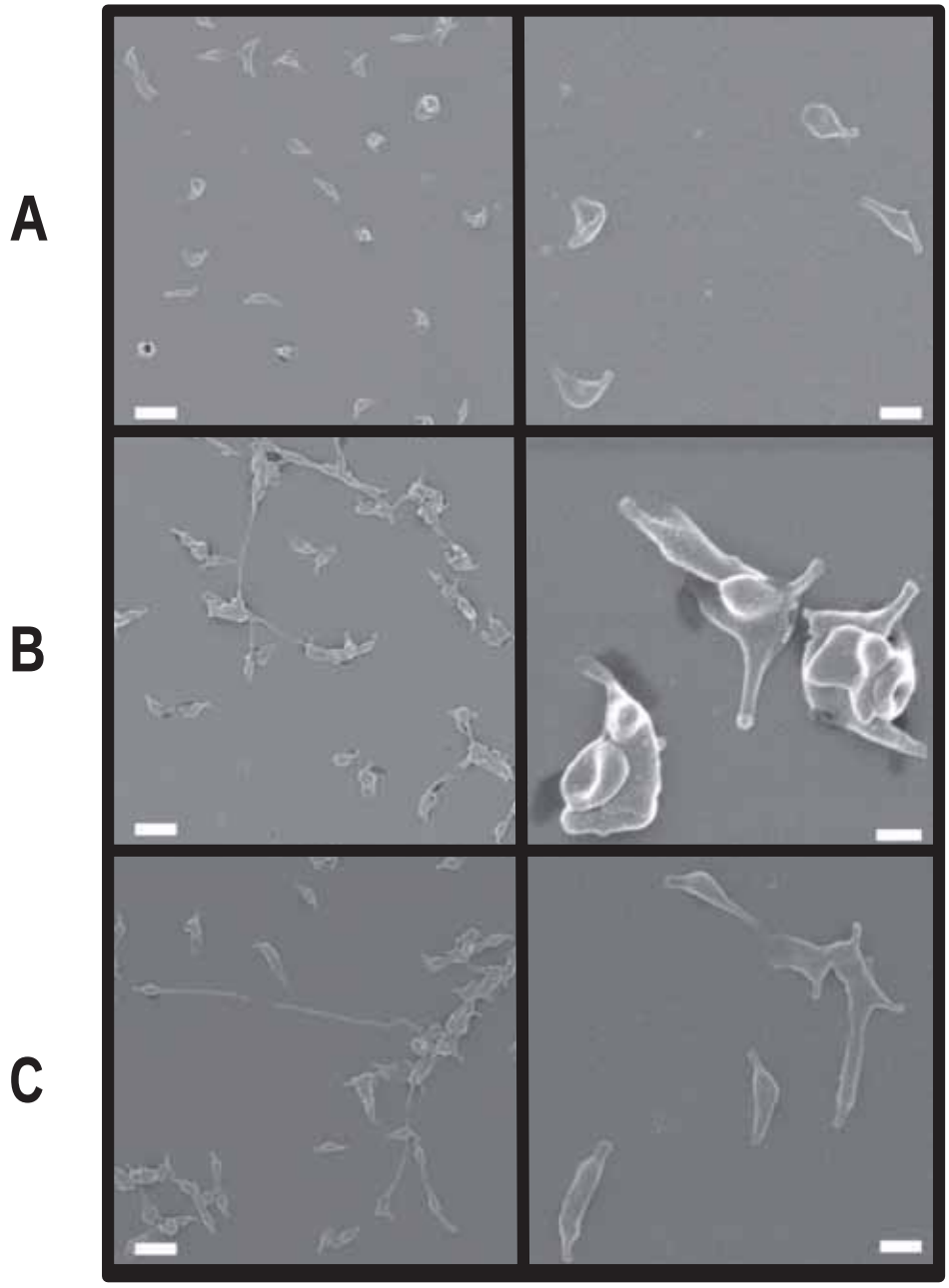

Figure 2.13. Scanning electron microscopy of WT and P32 related strains. Scale bar for right panels is 0.5 µm unless otherwise indicated. Scale bar for left panels is 1 µm. **A.** WT **B.** Δmg318. In right panel scale bar is 200 nm **C.** Δmg318C-ter **D.** Δmg318 + MG_318SP **E.** Δmg318C-ter + MG_318SP.

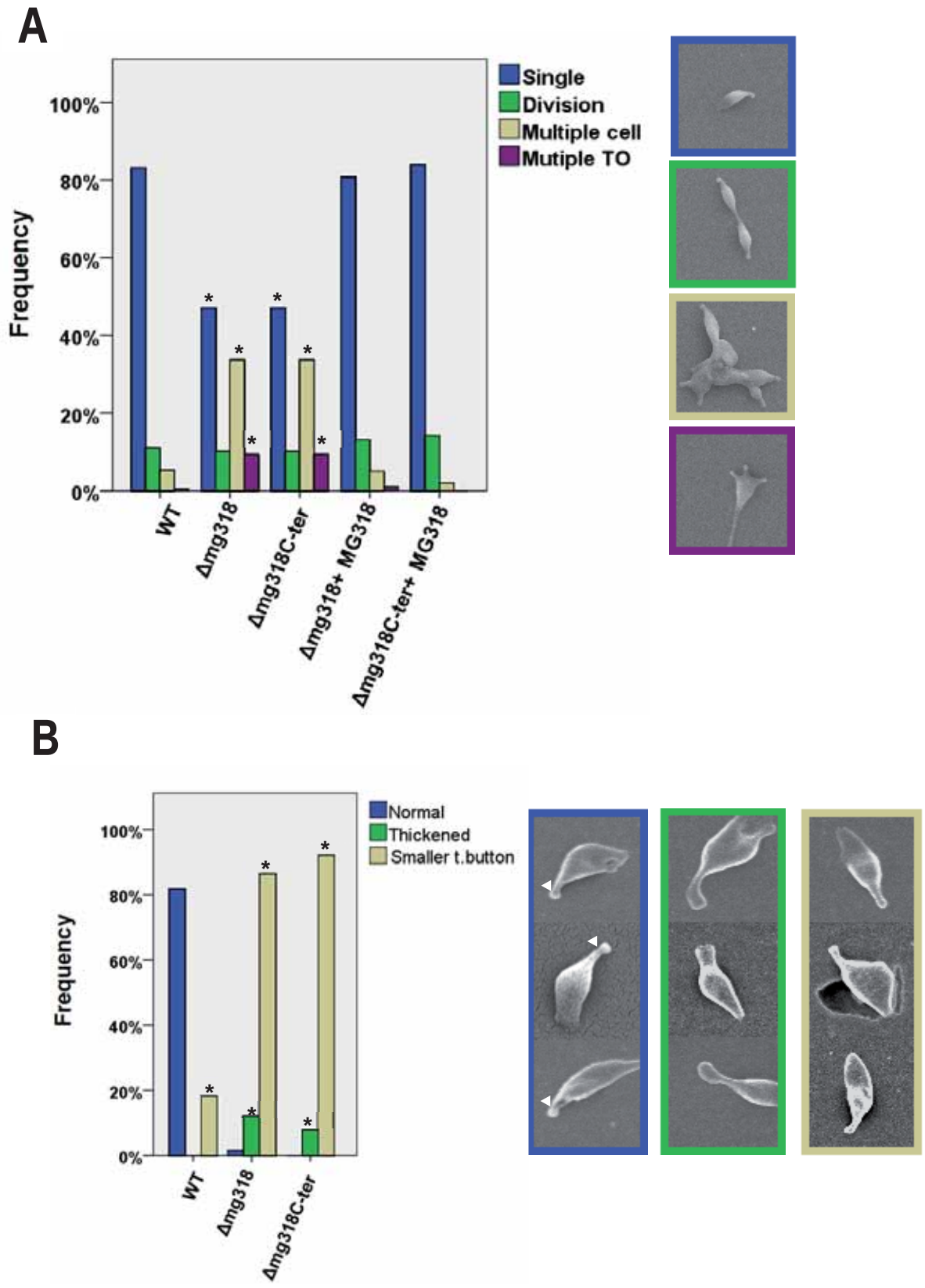

Figure 2.14. Cell division status and terminal organelle of WT strain and P32 mutant strains. The asterisk (*) indicates statistical significantly different when compared with the WT (p value < 0.01).Bulging at the tip of the terminal organelle is pointed with a white arrow.

5.3 Discussion

Although P32 homolog in *M. pneumoniae* has been profusely studied and established crucial for gliding—since no motile cells have never been observed—and this mutant completely recovers gliding frequency and speed after the reintroduction of either P30 or P32 one would expect a very similar phenotype in a mutant lacking P32. Surprisingly, this is not the case. In contrast, lack of P32 protein caused a significant decrease—72%—of the P110 and P140 main adhesins in *M. genitalium* cells but cells are still able to glide—at 61% of the velocity and 43% of the frequency. The null mutant for P32 protein and the mutant lacking the P32 C-ter presented the same gliding behaviour thus discarding a direct role of N-terminal of P32 in gliding motility. Both the null mutant strain and the C-terminal lacking strain did recovered WT phenotype. Confirming the role of MG318 in gliding motility and main adhesins stabilization.

It has been demonstrated in *M .pneumoniae* that P30 processing is critical for its function and the unprocessed form cannot be detected in the WT strain. In contrast, *M. genitalium* P32 protein mature and unprocessed forms seem to be in 1/3 ratio being more abundant the post-translationally processed form. This data suggest that P32 protein of *M. genitalium* is less efficiently processed than its orthologue in *M. pneumoniae*.

It was previously hypothesized that P30 is the gliding motor of species belonging to the *M. pneumoniae* cluster but the results in this chapter discard that hypothesis, at least, in *M. genitalium*. One could raise several explanations to explain the differences observed. First of all the frameshift mutation in mutant II-3 of *M. pneumoniae* could lead to an undetected 31.5 kDA protein which negatively impacts gliding motility. Secondly, it is possible that simply P30 of *M. pneumoniae* is responsible for more functions that P32 protein. Thirdly, it is important to note that the decrease in the amount of the main adhesins in mutant II-3 has been not been reported, and it is possible that the lack of P30 but steady-state levels of the main adhesins results in a non-motile phenotype. Another possible and simpler explanation is that that P1, P40 and P90—the orthologous proteins for P110 and P140- are far more stable in the absence of P30, and the downregulation/instability of P110 and P140 in P32 null mutant is a pure random fact, that at the end of the day, allows null mutant P32 cells to glide.

It is also important to emphasize the subtle changes in the terminal organelle of P32 null mutant strains. Almost the totality of the cells in P32 or P32 C-ter lacking strains no wild-type terminal organelles were observed. Most of them lack the bulging end characteristic of the terminal button and the rest of the cells present a thickened terminal organelle. The lack of the bulging end at the tip of the terminal organelle can also be observed in the SEM

micrographs obtained from ΔMG_217 strain (Burgos et al., 2008). MG217 protein is present at wild-type levels in strains lacking P32 suggesting an important role of both proteins in terminal button formation. It is also possible that P32 is not properly positioned in the absence of MG_217 or vice versa—similar to *M. pneumoanie* results suggesting that P65 truncation affects P30 localization(Hasselbring et al., 2012)—but it seems that this is more experimental data is needed in order to explore that hypothesis in *M. genitalium*.

The long filaments observed in the multiple cell aggregates have been not previously described in any strain of mycoplasma (natural or genetically engineered) thus suggesting a more important role of P32 in cell division that previously envisioned. To further analyse this hypothesis growth curves of all strains in this chapter should be performed.

Unfortunately, the reduced levels of P110 and P140 in either ΔMG318 or ΔMG318C-ter difficult the fact to stablish the sole role of P32. Luckily, a mutant of *M.genitalium* with reduced levels—and similar amounts—of P110 and P140 proteins have been previously characterized. Since no affectation other than cells multiple terminal organelles have been observed in this strains, all the other phenotype perturbation observed can be attributed to P32 the lack of P32 or the C-terminal or P32. In fact, the most reasonable explanation why cells of ΔMG318 and ΔMG318C-ter strains present multiple terminal organelles is that it is caused by the reduced amounts of P110 and P140.

The results obtained in this chapter do not allow to reach any direct conclusion about the functionality of P32 N-terminal domain. However, almost no clones isolated using pΔMG318C-ter plasmid showed the total loss of P110 and P140 adhesins but half of the mutants obtained using pΔMG318 showed that loss. In addition, all of the isogenic strains lacking P32 presented a 60% in the protein levels of P110 and P140 but isogenic strains lacking the C-ter of P32 showed adhesion levels ranging from 40% to 60% of those from the WT. Whole genome sequencing showed no big differences between genomes—except for small heterogeneities in the coding regions of P110 and P140—and may explain those differences. However, the molecular origin destabilization is unknown.

This suggests an undefined role of the N-terminal of P32 protein in the stabilization of P110 and P140. In the moment of P32 disappears from the cell after the double recombination event takes place and also a role in the stability of the main adhesins after the deletion of the C-terminal of P32. The most feasible explanation why strains lacking P32 and also lacks P110 and P140 is that recombination events in the MgPa islands with the MgPa operon have taken place—losing its capacity to encode functional P110 or P140—as suggested by the NGS results. The reason why only near 50% of the recovered clones after transformation with

pΔMG318 suffered this alteration is not clear, since strains not lacking P110 and P140 does not seem to present an increased variability—therefore in recombination frequency—of these regions.

6. Chapter III: Functional analysis of the high molecular weight protein MG386

6.1 Introduction

6.1.1 Previous knowledge of MG386 protein

MG386 protein is a 186 kDa with higher apparent Mw on SDS-PAGE gels—300 kDa. This protein contains five EAGR box domains which have been previously linked to motility in other terminal organelle proteins(Calisto et al., 2012). Strains carrying transposon truncated forms of MG386 protein has been previously characterized (Pich et al., 2006, Pich et al., 2009). Transposon mutants of this protein showed a gliding speed of 30% when compared with the WT and a high frequency of cells showing trembling movement. Micro-cinematographic analyses showed that the largest it is the portion of the protein that remains intact after the transposon insertion, the greater the gliding frequency. Isolated mutants showed a ratio of gliding cells between 20% or 47% depending on the insertion site of the transposon. Inversely, the ratio of trembling cells varied from 67% to 46%. Similarly, the null mutant of orthologous protein P200 in *M. pneumoniae* showed a gliding speed of 30 % of the wild type and an increase of a 20% of the non-motile cells.

It has been also observed that MG386 protein is dramatically destabilized in strains lacking P110 and P140, but the opposite effect have not been observed (Burgos et al., 2006). In addition to the fact that the C-terminal region of MG386 strongly interacts with the C-terminal of MG219 (Martinelli, 2014), it has also been demonstrated that MG386 localizes in at a similar distance to MG318 protein and the cell body that MG219, making its localization compatible to be assigned to the wheel complex (Fig. 3.1) (Mariscal AM, manuscript in preparation).

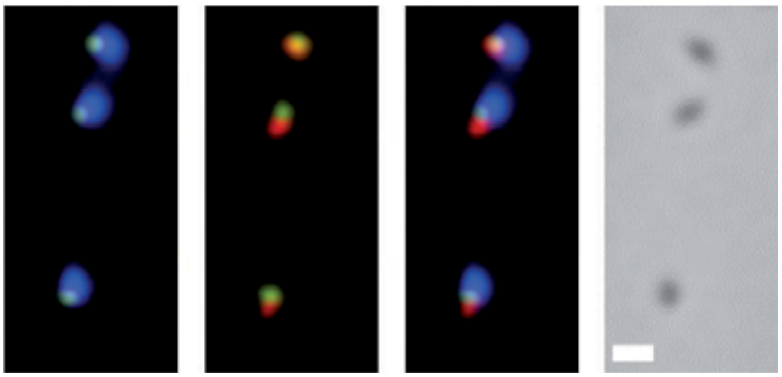

Figure 3.1. Subcellular localization of MG386. Blue: DNA. Yellow: MG386. Red : P32

6.2 Results

6.2.1 Obtaining MG386 mutants

In order to obtain a mutant lacking the MG386 protein by homologous recombination, plasmid ΔMG386 was created (Fig 3.2A). The LHR of this plasmid contains a 1007 bp upstream of MG_386 start codon and RHR contains the 1000 pb downstream of MG_386 locus. RHR homology region also contains the last 144 pb of the MG_386 in order to maintain the possible promoter region of the downstream gene MG_385.

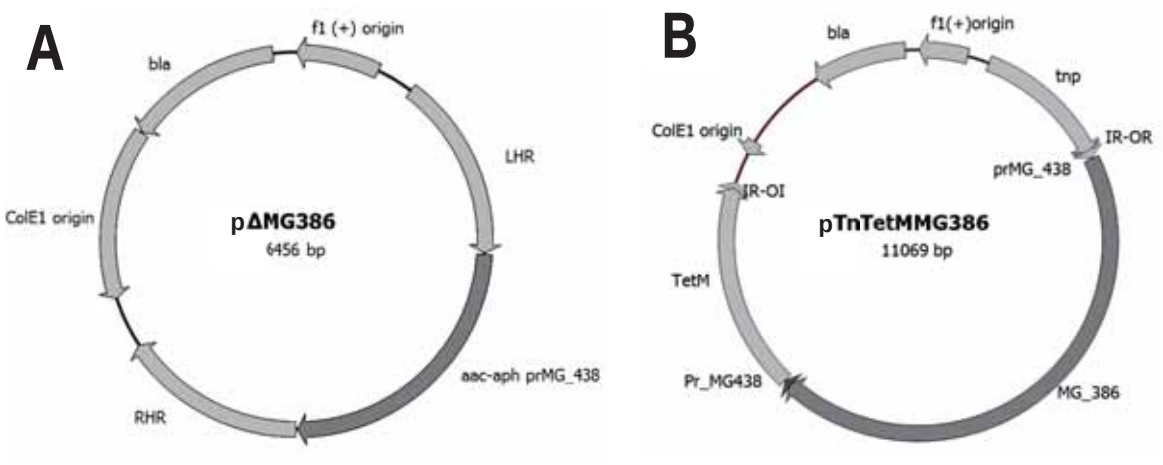

Figure 3.2. Schematic representation for the deletion of MG386 by homologous recombination or the random insertion of MG386 by transposition. **A.** pΔMG386. **B.** pTnTetMMG386.

For later complementation studies, plasmid pTnTetMM386 was created (Fig. 3.2B). This plasmid harbours MG_386 gene under the control of the 438 promoter. Upon introduced in a null mutant it is expected that this copy will be able to restore the WT of MG386 protein.

6.2.2 Confirmation of MG386 related mutants

Since MG386 is the highest molecular weight protein visible by Coomassie blue staining and does not overlap with any other band, initial mutant confirmation was carried analysing the protein profiles by SDS-PAGE of the cells transformed with pΔMG386. Unluckily, the transformation efficiency of this plasmid was shown to be extremely low ($1 \cdot 10^{-8}$ mutants per viable cell), which is 50 times lower than the previously reported efficiencies for homologous recombination (Burgos et al., 2006). The sole colony recovered was named Δmg386. The origin of such low transformation efficiency is unknown, but correlates well with previous attempts in our lab of obtaining this null mutant (unpublished results). The only clone recovered after transformation with pΔMG386 was electroporated with pTnTetMMG386 obtaining strain Δmg386 + MG386.

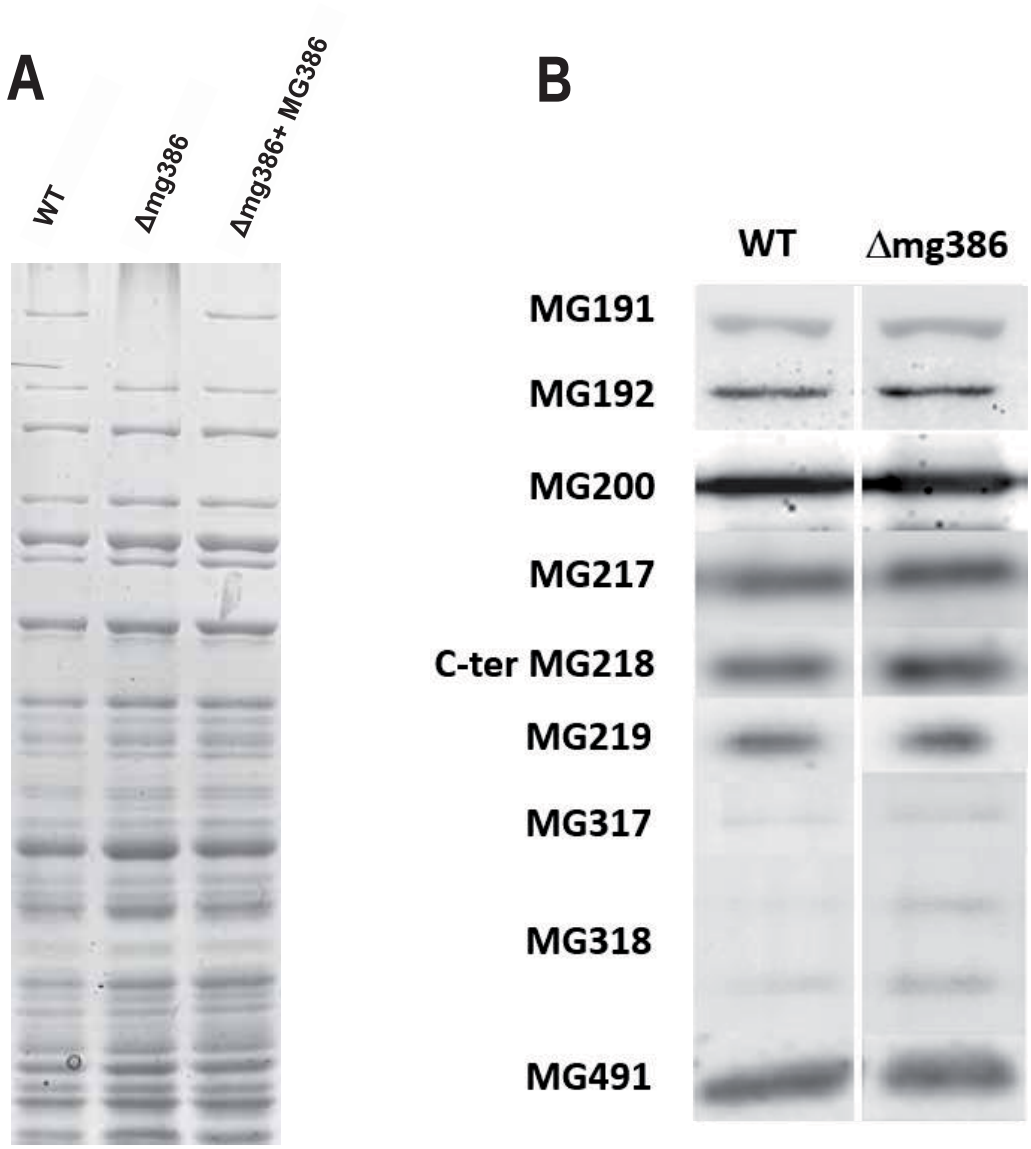

Figure 3.3. Protein levels of the WT strain and MG386 mutant strains. **A.** The upper band—corresponding to MG386—is clearly not apparent. This band correspond to MG386 protein (Pich et al., 2006). B. Western blot using antisera against most of the known proteins of the terminal organelle.

Both Δmg386 and Δmg386 + MG386 mutant's strains behaved as previously expected. The corresponding band to MG386 disappeared in MG386 strain but reintroduction of the WT MG_386 allele promoted the recovery of MG386 wild-type levels (Fig. 3.3A). Western blot analyses revealed no major effects on other proteins responsible for the functioning or structure of the terminal organelle (Fig. 3.3B).

Deep sequencing of ΔMG386 confirmed that this strain carries the intended gene mutation. Comparison of the reads obtained by Illumina Sequencing with the genome of the wild-type strain revealed that no copies—or fragments of—MG_386 are present in the genome of ΔMG386 strain (Fig. 3.4A). In agreement with that, alignment of the sequences with the

expected ΔMG_386 genome revealed that the intended gene replacement was performed without extra relevant mutations (Fig. 3.4B, appendix 12.4).

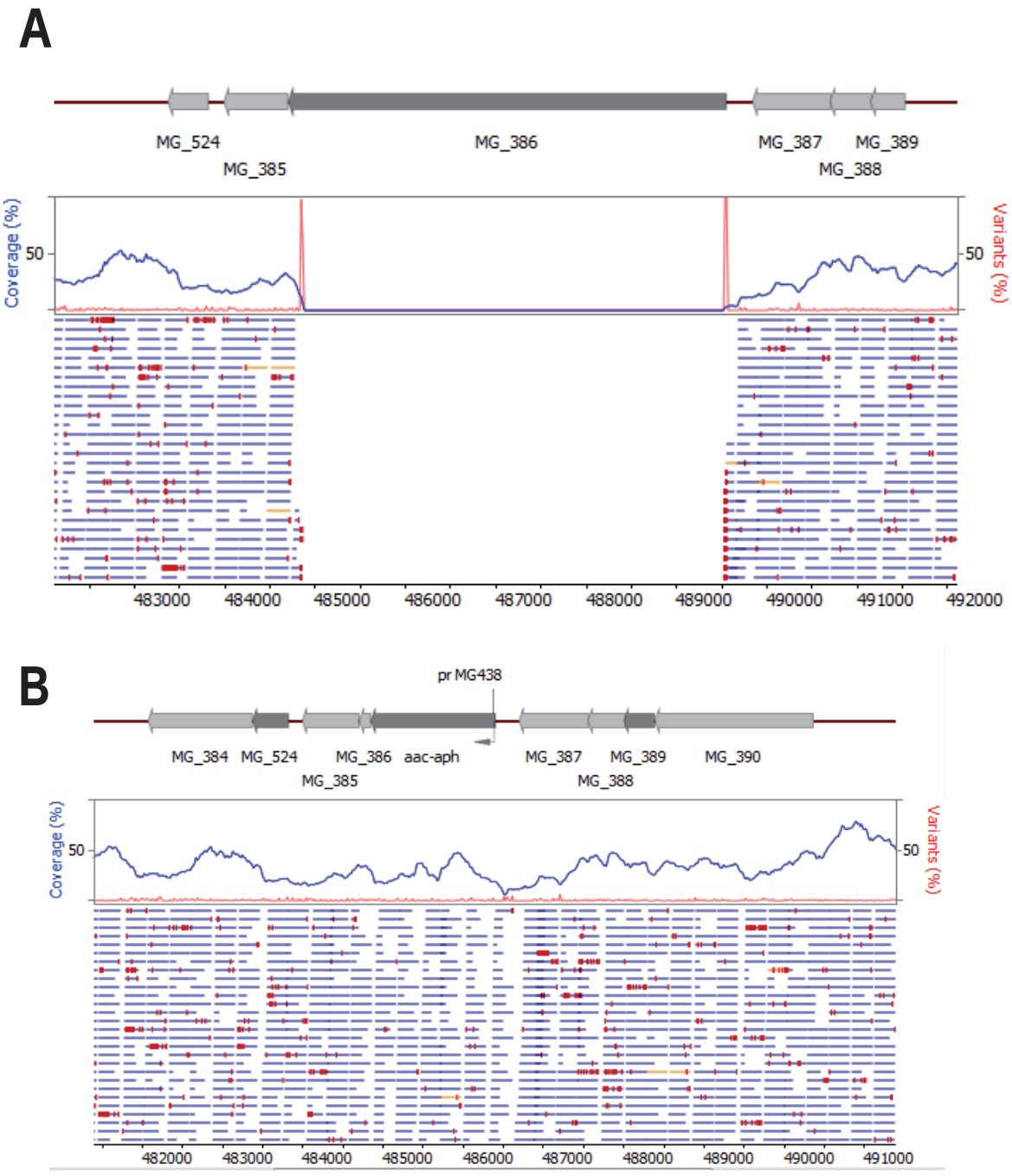

Figure 3.4. Region of the whole genome analysis of Δmg386 strain. **A.** Comparison with the genome of G37 wild-type strain. **B.** Comparison with the theoretical genome of Δmg386 strain. The numbers indicate base numbers of reference genome used.

6.2.3 Characterization of MG386 mutants

6.2.3.1 Gliding motility

Qualitative gliding motility measurement showed a huge number of non-motile cells in Δmg386 strain, the presence of very narrow circular tracks is also apparent (Fig. 3.5).

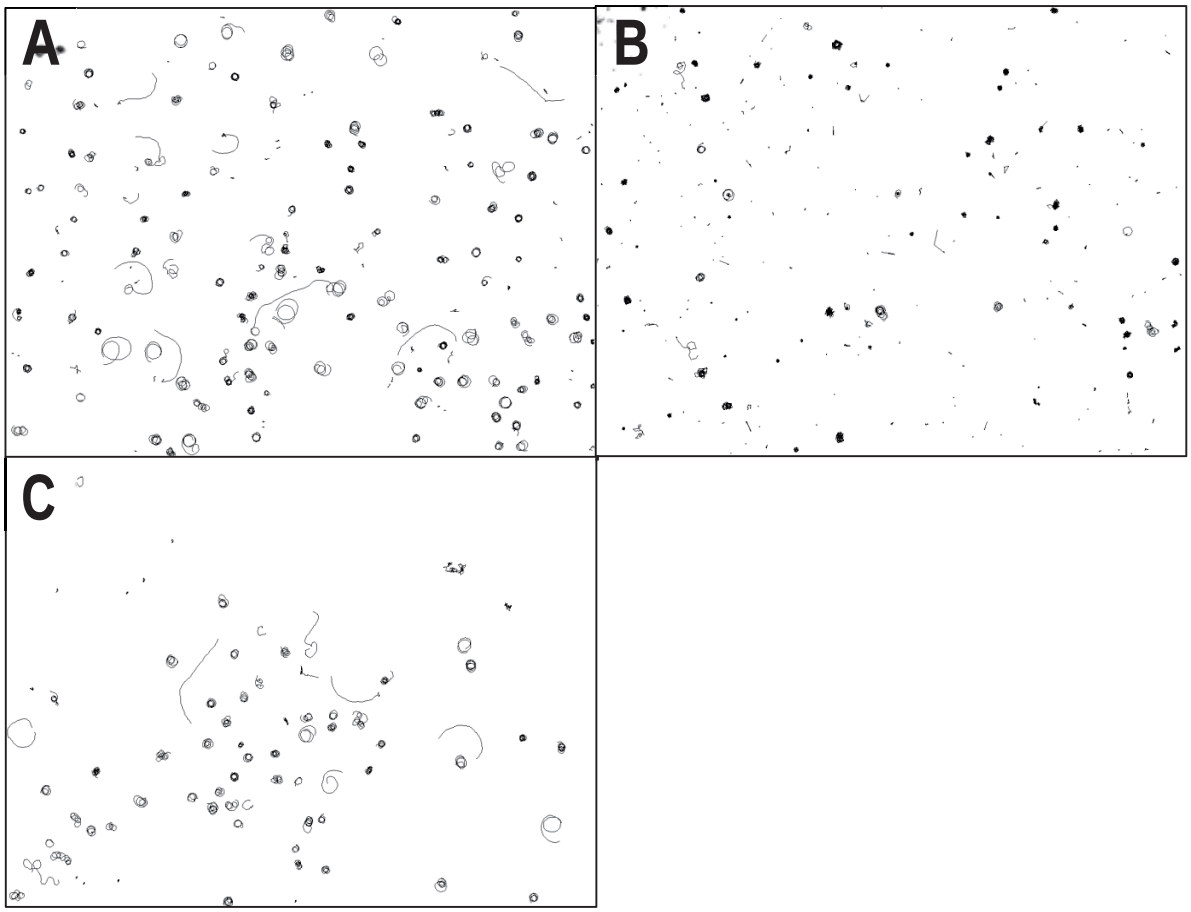

Figure 3.5. Paths depicted by MG318mutant strains in comparison with WT strain during a period of two minutes at 37ºC in SP4 medium. **A.** WT **B.** Δmg386 **C.** Δmg386 + MG386. Each image shows a region of 86.9x65.2 µm.

When quantitative analyses were performed, important differences in all the gliding parameters were observed (Fig. 3.6). A dramatic decrease of 10% of erratic paths was observed in Δmg386 strain, thus virtually all cells (99%) were moving depicting circular tracks (Fig. 3.6A). In addition, Δmg386 strain showed a decrease of a 44 % in gliding frequency (33% vs 77%) (Fig. 3.6B). When the diameter of the circular tracks depicted on moving cells was assessed, a decrease of a 35% of its diameter was observed—0.67 ± 0.03 µm vs 1.02 ± 0.06 µm (Fig. 3.6C). Extraordinarily, an increase of a 70% in gliding speed (0.170 ± 0.010 µm s^{-1} vs 0.118 ± 0.004 µm s^{-1}) when compared with the WT is noticed (Fig. 3.6D).

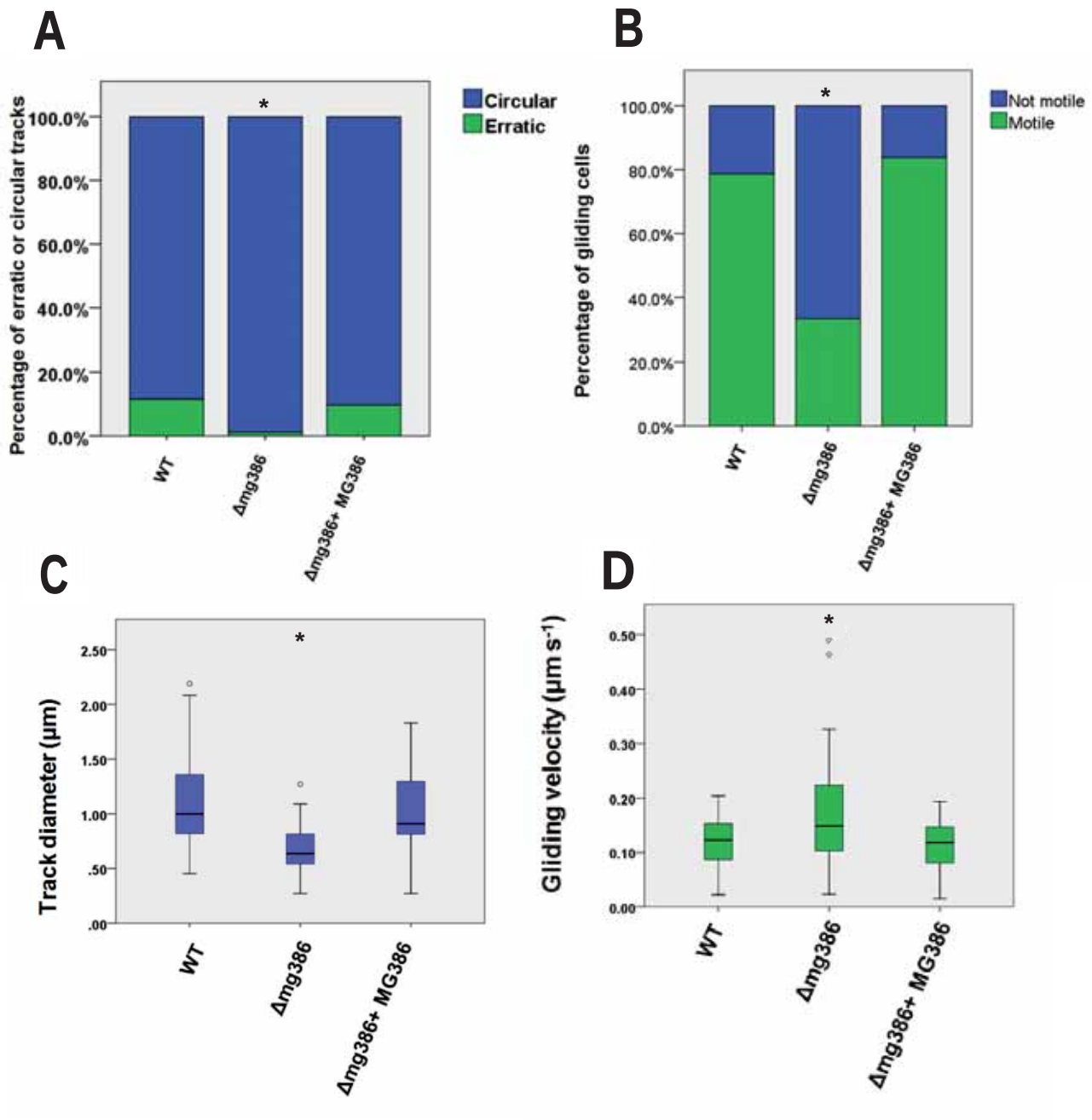

Figure 3.6. Gliding properties of WT and strains with modifications related to MG_318. **A.** Frequency of erratic and circular tracks **B.** Frequency of motile and non-motile cells **C.** Boxplots of gliding velocity. The number sign (*) indicates statistical significantly different when compared with the WT (*p*-value < 0.01).

Fascinatingly, minute cells—almost impossible to distinguish by phase contrast microscopy—are also visible in micro-cinematographic studies of Δmg386 strain, some of them performing gliding motility (Fig. 3.7B).This cells were treated separately from bigger cells in quantitative and statistical analyses. Minute cells glide at a 0.082 ± 0.008 μm s^{-1}—69 % of the wild-type—(Fig. 3.7A). In spite of this, a small fraction of minute cells are capable to glide around wild-type speed. Gliding frequency these minute cells is 16.5 % which is even slower than the Δmg386 strain. Such differences resulted to be statistically significant when compared with the wild-type strain and the standard-sized cells of Δmg386 strain. The global impact of this minute cells in gliding statistics are negligible since minute cells represent only 11% of the total cells. Adding those minute cells to the previous statistical analyses resulted in no differences in the changes observed between the wild-type strain and Δmg386 strain data not shown). No minute cells were observed in Δmg386 + MG386 strain, and all other gliding parameters showed no differences with the WT strain. The frequency values for non-motile minute cells should be treated carefully since it is very difficult to differentiate debris from minute cells.

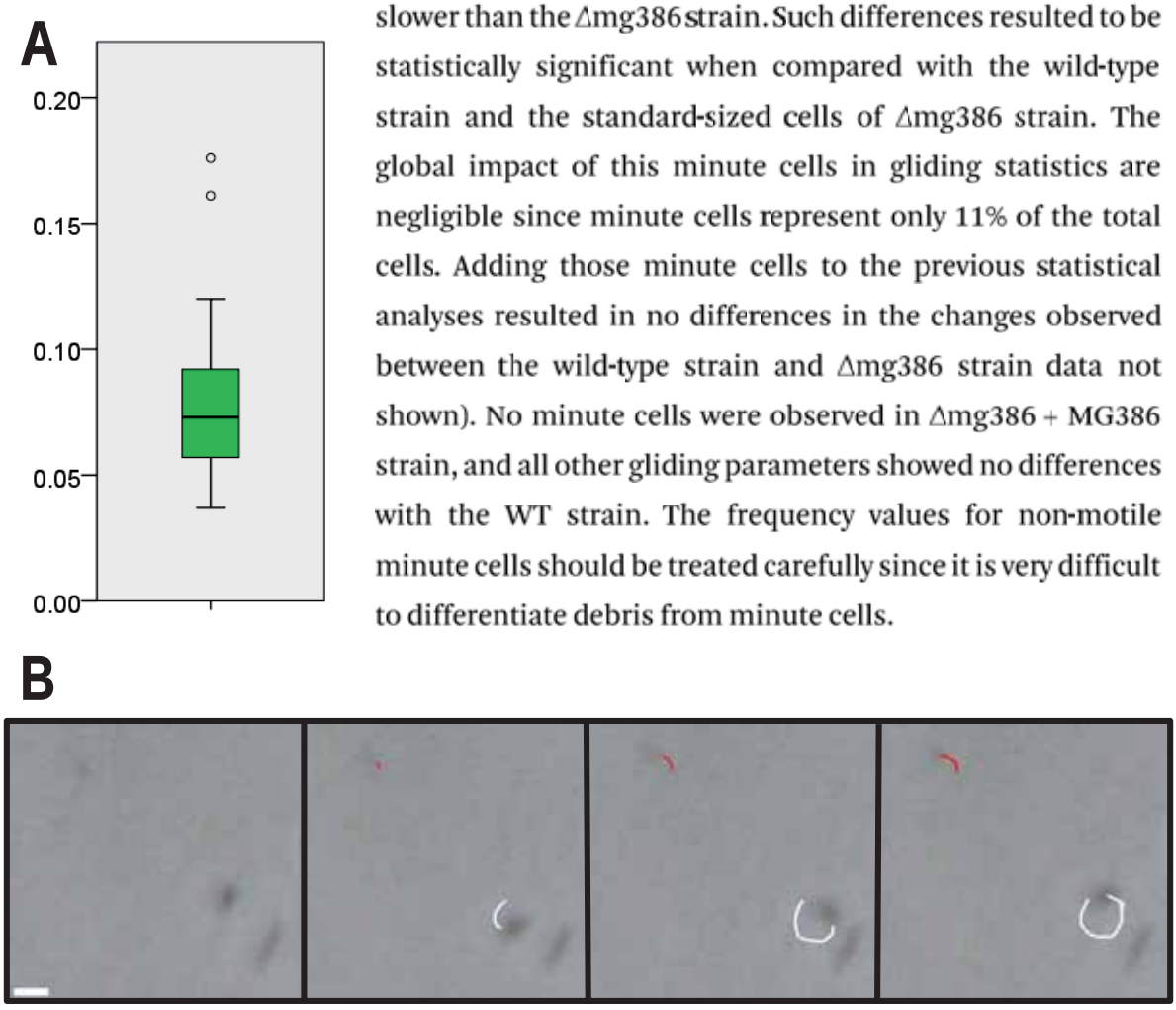

Figure 3.7. Gliding motility of minute cells present in Δmg386. **A.** Boxplot of Δmg386 gliding velocity **B.** Time-lapse phase contrast microscopy of Δmg386 cells. The red track arises from a minute cell. The white track arises from a WT-sized cell. Scale bar is 1 μm.

6.2.3.2 Cellular morphology

Scanning electron microscopy of Δmg386 strain showed striking differences with the wild-type strain. The first big difference is the high number of large aggregates suggesting problems in cell division caused by the absence of MG386 protein (Fig. 3.8). It is also remarkable the high prevalence of protruding filaments from those aggregates or filamentous cells that seem to have been detached from those aggregates and are able to glide across the solid surface. In some cases only the tip of the filament—the terminal organelle—is able to detach from the aggregates, forming in this way minute cells. The frequency of minute cells in SEM is 10.3%, which is compatible with the phase-contrast results. It is important to note the relative high prevalence of cells without an observable terminal organelle, most likely due to the detachment of the TO from this cells. Measurement of the minute cell sizes showed this cells to be 300 nm large x 100 nm wide.

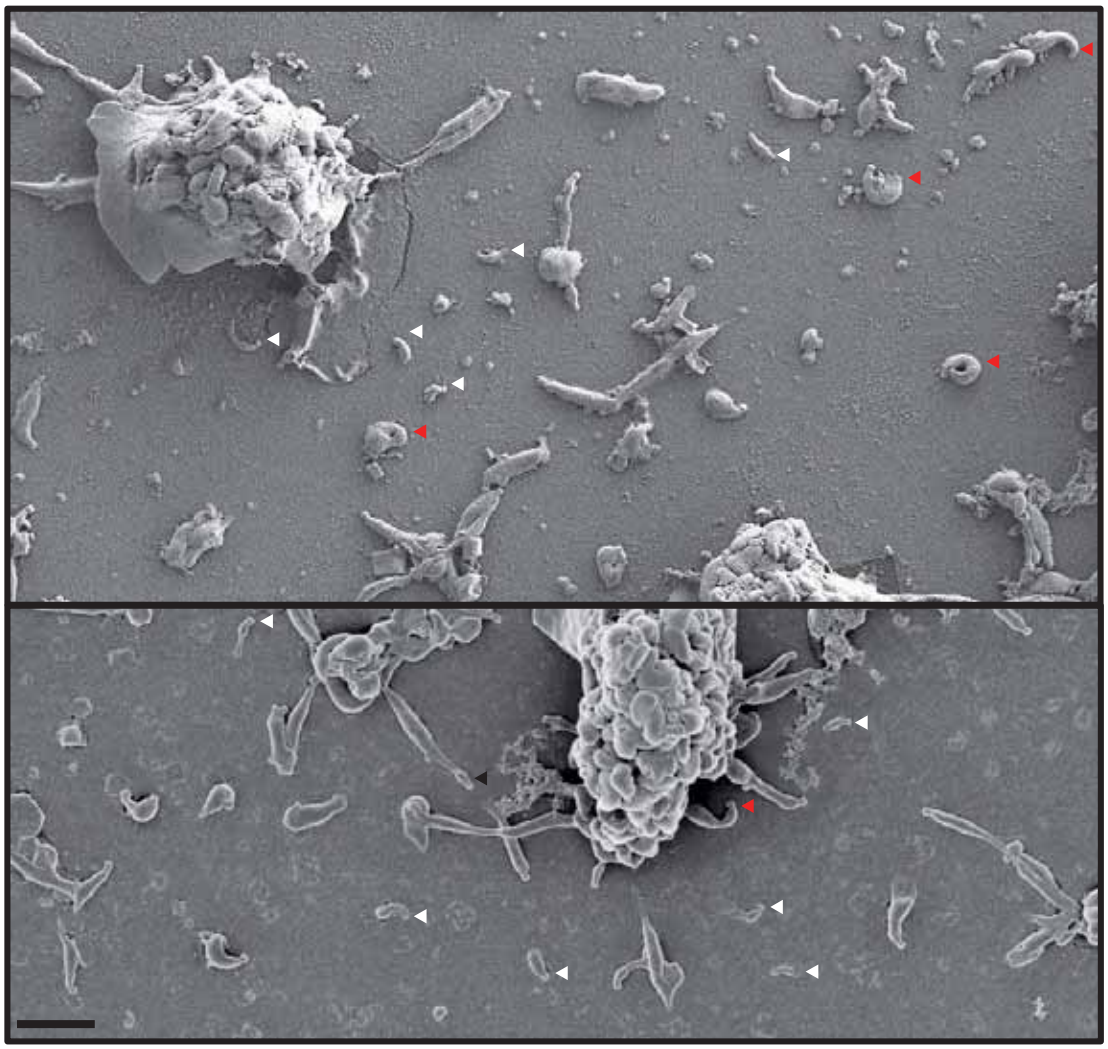

Figure 3.8. Scanning electron microscopy of MG386 strain fixated in SP4 medium. Minute cells are pointed with a red triangle. Cells showing an uncommon crooked terminal organelle are pointed with red arrows. Minute cells are pointed with white arrows. Black arrow point to a minute cell in formation due to a detachment. The sample is dirtier than the ones showed in chapter I and II since fixation of the cells was carried out with media to avoid losing minute cells or filament breaking. Scale bar is 1 µm.

From cells presenting the standard flask shape morphology, it is noteworthy the high prevalence of cells presenting extremely crooked terminal organelles, some of them even touching the trailing part of the cell. Those cells present a similar morphology to the bipartite cells previously described for the defective in a small region in the C-ter of MG491 (Martinelli et al., 2015).

6.3 Discussion

A null mutant of MG386 protein has been obtained and characterized. This protein has shown to be critical for maintaining wild-type gliding properties *M. genitalium*. Remarkably, all the parameters analysed—gliding behaviour, diameter of the circular tracks, gliding frequency and gliding velocity—were affected. The most evident phenotype when observing the cells at the phase contrast microscope is that those cells glided faster than the wild-type. In fact, the cells are gliding so fast that it is possible that the real value of gliding speed is undervalued, since the circular tracks are not well depicted in the time-lapses of two seconds performed. The second most evident phenotype is that there are almost no cells presenting erratic tracks and the circular ones are extremely narrow. Electron scanning microscopy showed that this narrow tracks are caused—or are consequence—of crooked cells that lead to head-to-tail morphology in the most extreme cases. It was also striking the appearance of filamentous cells and minute cells. The most reasonable explanation for the generation of minute cells is that the filaments are generated by gliding motility and, at the end, the filament or the terminal organelle detaches and starts gliding on his own, similar to the phenotype observed in P41 mutant of *M. pneumoniae*. This view will be confirmed in chapter IV.

Interestingly, a mutant lacking a small peptide within the C-terminal region of MG491 have shown present also minute cells, crooked cells and smaller diameter circular tracks (Martinelli et al., 2015). Being both MG491 and MG386 proteins in the wheel complex, it is possible that an undefined interaction between the C-terminal of MG491 and MG386 is critical for MG386 functioning.

Cells without terminal organelle could explain, at least in part, the reduced levels of motile cells in this strain. It is likely that the filamentous aggregation-prone tendency of the cells of this strain explain the rest of the non-motile cells.

All these data taken together suggest that MG386 protein is a negative regulator of gliding motility and/or is critical for the proper anchoring of the terminal organelle to the cell body.

With the experiments performed it impossible to discern whether detachment is a cause or a consequence of MG386 loss. If MG386 is key for anchoring the terminal organelle to the cell body, it is possible that terminal organelles detach just for lack of anchoring. But if MG386 is a negative regulator of gliding motility velocity and strength its elimination may result in a major propulsion helping terminal organelles to detach. Since flask-shape standard sized cells are able to glide at wild-type or even greater velocities—some extreme rare cases glides 4 times faster than the WT strain—it suggests that the greater velocities are a consequence of the absence of the proper transmission of the movement generated by the TO to the cell body.

It is possible to hypothesize that the friction and drag forces existing in the extracellular matrix—where *M. genitalium* performs its parasitic function—is higher than *in vitro* conditions. This increased resisting motion force could result in a rise of the frequency of detached terminal organelles. These situation would leave a high frequency of non-motile cells incapable to evade the hosts defence mechanisms and also incapable to further proceed the infection process. Such handicapped strains will be rapidly obliterated by selective pressure.

Δmg386 strain minute cells glide at 0.082 μm s^{-1} while standard-sized cells glide at 0.170 μm s^{-1}. Taking account of the second Newton's law this difference is at first glance surprising. Since the gliding machinery should be within the terminal organelle, it would expected to find that the higher the mass of the body to move, slower the measured velocity. Given that this is not happening, it means that the gliding machinery is not equally efficient when detached from the cell body. Two possible explanations are the most feasible for this phenomenon. The first one is that there is some active part of the machinery within the cell body that aid the cells to propel themselves at such high speeds. The second one is that the terminal organelle is fully functional but it needs a constant source of energy (NTPs, membrane potential, etc.) and in the moment when it detaches this continuous flow of energy is broken, slowing the cells in the process. The fact that most of the minute cells—83.5%- are not performing gliding partially supports the second theory because, eventually, the energy source would have been completely exhausted thus stopping the terminal organelle function.

Unluckily, results found in this chapter do not explain the instability phenomenon taking place in null mutants for P110 and P140 proteins. Preceding the results showed in this chapter, the reason why MG386 transposon mutant strains did not show also reduced levels of MG386 was unclear. The most reasonable explanation was that the N-terminal of MG386 was responsible of interacting or stabilizing P110 and P140. This has been not proven truth

since the null mutant for MG386 did not show altered levels of the main adhesins demonstrating that the destabilizing phenotype is unidirectional. Given the MG386 function described in this chapter the underlying reasons of this process remains elusive.

Lastly, it is difficult to explain the differences observed between mutants harbouring a transposon within the coding region of MG386 previously reported. The most feasible explanation is that the N-ter of MG386 plays a key role in most of the processes described in this chapter but more convincing data should be found to demonstrate this hypothesis.